Origin and geometry of upward parallel electric fields in the auroral acceleration region

F. S. Mozer and A. Hull

Space Sciences Laboratory, University of California, Berkeley

Abstract. Electric fields, magnetic fields, and plasmas measured on the Polar satellite are studied to determine the altitude extent of the upward field-aligned current portion of the auroral acceleration region and the physical processes that populate it with parallel electric fields. This region extends upward to a geocentric altitude of 3 or 3.5 Earth radii at premidnight local times during the spring and fall. In a model for this region a necessary but not sufficient condition for the appearance of parallel electric fields is an upward field-aligned current. Parallel electric fields will exist where the plasma density is insufficient to carry this imposed field-aligned current through the converging magnetic field. These parallel fields are associated with (1) high-altitude electron acceleration required to carry the imposed current through the low-density region; (2) a low-altitude sheath required to inject compensating positive charge into the region and to restrict entry of secondary electrons from below; and (3) the midaltitude maintenance of local charge neutrality. The parallel electric field in the low-altitude sheath is directly measured to be as large as several hundred mV m^{-1}, while the higher-altitude fields appear to have magnitudes of a few mV m^{-1}. The low-altitude sheath is corrugated in a manner that does not depend on striations of the field-aligned current but that may depend on density variations.

1. Introduction

The existence of parallel electric fields in the auroral acceleration region was first suggested by electron spectra measured on a sounding rocket [*McIlwain*, 1960]. This interpretation was strengthened by *Evans's* [1974] explanation of low- energy electrons observed on sounding rockets as being secondaries produced by auroral primary electrons and reflected by the parallel potential above the sounding rocket [*Evans*, 1974]. The initial particle evidence was completed by the first observation of upgoing ion beams on the S3-3 satellite [*Shelley et al.*, 1976] and upward acceleration of a barium ion cloud [*Haerendel et al.*, 1976].

The first direct electric field evidence of parallel electric fields in the auroral acceleration region was made on the S3-3 satellite through observation of very large (~1000 mV m^{-1}) perpendicular electric fields, called electrostatic shocks [*Mozer et al.*, 1977]. Parallel electric fields were required to explain why these fields did not map to the ionosphere, where such large fields are not observed. The S3-3 satellite also made direct measurements of parallel electric fields of hundreds of mV m^{-1} [*Mozer et al.*, 1980]. Such measurements had small impact on the field, perhaps because they were not put into context by simultaneous plasma and field-aligned current measurements. It is the purpose of this paper to put such measurements into this context by examining particles and fields observed on the Polar satellite during several hundred passes across auroral zone magnetic field lines at geocentric altitudes of 2-6 Earth radii. These passes all occurred in the spring or fall and at magnetic local times of ~2000-2400.

The Polar satellite was launched on February 24, 1996, into an elliptical polar orbit with apogee of ~9 Earth radii geocentric over the North Pole and a perigee of ~2 Earth radii. Through rotation of its line of apsides with time, Polar has traversed auroral zone magnetic field lines in the premidnight meridian at all altitudes between perigee and near apogee. As part of the payload, Polar

carries a three-axis electric field instrument [*Harvey et al.*, 1995], a magnetometer [*Russell et al.*, 1995], and the HYDRA plasma instrument [*Scudder et al.*, 1995]. The data from these instruments will be used in this paper to discuss the auroral acceleration region.

2. A Model

To cast previous knowledge and the data presented in this paper into a unified framework, a model of equipotential contours in the auroral acceleration region is illustrated in Figure 1. The only assumption of this model is that the boundary condition imposed on this region is an upward field-aligned current. This is a zeroth-order model that ignores the effects of waves and considers only DC parallel electric field effects. The magnetic field lines are vertical in the meridional plane illustrated in Figure 1. The illustrated equipotential contours represent one of an infinite number of such contour plots that are consistent with experimental data. The features of the data that are required in any such model and that define the low-altitude boundary of the acceleration region are discussed next.

2.1. Low-Altitude Boundary of the Auroral Acceleration Region

The low-altitude boundary (found at 2.0-2.5 geocentric Earth radii) is corrugated with fingers of potential extending to lower altitude, such as that illustrated in Figure 1. A spacecraft passing below the lowest potential finger will observe the relatively high-density ionosphere, downgoing inverted-V electron distributions, no upgoing ion beams, and an electric field consistent with that in the ionosphere. A spacecraft flying through a finger will cross boundaries containing large perpendicular fields, and, if the potential contours are inclined with respect to the magnetic field, a large parallel electric field. Within the potential finger or just above the low-altitude boundary, the plasma density is low because there is little or no cold plasma (essentially all of the plasma has been accelerated to carry the field-aligned current), the electric field is turbulent, there is an upgoing ion beam whose energy is given by the perpendicular potential difference, and there are downgoing accelerated electrons. These properties are illustrated elsewhere [*Mozer and Kletzing*, 1998; *McFadden et al.*, 1999].

The Polar satellite has traversed thousands of potential fingers at geocentric altitudes near 2 Earth radii and has measured ~50 examples of significant (greater than 10% of the perpendicular field), upward directed, parallel electric fields at their boundaries. One example of such fingers and a measured parallel electric field is illustrated in Plate 1. Plates 1a-1c are the electric field components in a magnetic field oriented coordinate system. Plate 1a is the perpendicular electric field component in the magnetic meridional plane and pointing equatorward, Plate 1b is the perpendicular field component in the magnetic westward direction, and Plate 1c is the parallel field. Plate 1d is the spacecraft potential, which is a measure of plasma density and which shows that the plasma density varied from ~0.01 to 10 particles-cm3 during this 45-s interval [*Scudder et al.*, 2000]. Plate 1e is the integral of the measured perpendicular electric field along the spacecraft trajectory, and the Plate 1f is the westward component of the magnetic field that is perpendicular to a model magnetic field line. Its slope gives the strength of an assumed field-aligned current sheet, which is

upward for the negative slope in Plate 1. (The slope of the westward magnetic field corresponding to an upward field-aligned current depends on whether the spacecraft moves southward or northward through the current. In this paper, data are presented from May and November time frames, at which times the spacecraft moved southward and northward, respectively, through the upward field-aligned current. Thus, for an upward field-aligned current the slope of the westward magnetic field is negative in the May data and positive in the November data.) Plates 1g-1j give the differential energy flux of upgoing ions, downgoing ions, upgoing electrons, and downgoing electrons, respectively, where all distributions are for particles within 30× of the magnetic field line.

Two potential fingers were crossed in the data of Plate 1. They appear within the intervals 2251:01-2251:04 and 2251:20-2251:39 universal time. Before, between, and after the fingers the electric field was small and consistent with an ionospheric value. Within the fingers the perpendicular electric field was as large as 750 mV m^{-1}, and it was turbulent. A parallel electric field of up to 250 mV m^{-1} was observed near the boundary of the first finger. It was positive (upward) as is required for this upward current region. In the second potential finger the parallel electric field was consistent with zero, as it is in most finger crossings. The plasma density decreased by a factor of more than 100 in the first finger and more than 10 in the second.

The field-aligned current (Plate 1f) was roughly constant through the time interval, and inverted-V electrons were observed all of this time (Plates 1i and 1j). Within the fingers and not elsewhere, upward ion beams were observed at every measurement opportunity (Plate 1g). The ion beam energies were consistent with the potential differences measured along the spacecraft trajectory (Plate 1e) and the assumption that the large perpendicular potential observed at the spacecraft became a parallel potential below the spacecraft, as illustrated in Figure 1. The ion beam energy was about a factor of 3 less than the electron energy, which shows that most of the parallel potential was above the spacecraft near the low-altitude boundary even though the parallel field in this region was large.

It is emphasized that in this example and most others there is little or no correlation between the strength of the field-aligned current and the presence or absence of potential fingers. Thus the potential fingers are not caused by striations in the field-aligned current.

A second example of low-altitude potential fingers is illustrated in Figure 2. Figures 2a and 2b give raw electric field measurements made by the two pairs of spin-plane booms that have sphere-to-sphere separations of 100 and 130 m, respectively. The small amplitude sine waves in Figures 2a and 2b are caused by the rotation of the detector in a relatively constant, ~15 mV m^{-1} field. The three potential fingers are characterized by large and turbulent electric fields. The spacecraft crossed the borders of each of the three potential fingers in a single data point (25 ms), so the boundary of the finger region is no wider than a few hundred meters at the spacecraft. As in Plate 1, the plasma density inside the fingers decreased by factors as great as 10 (Figure 2c) and the presence or absence of the potential fingers was not controlled by the magnitude of the field-aligned current (Figure 2d).

In summary, the key features of the low-altitude acceleration that are included in the model of Figure 1 and that are needed to

discuss the origin and geometry of the higher-altitude parallel fields are as follows: (1) The electron density inside the acceleration region is low in the sense that it is composed of mainly accelerated electrons. (2) Most of the parallel potential is above the low-altitude acceleration region. (3) The parallel electric field in the low-altitude acceleration region is significant, sometimes as large as hundreds of mV m^{-1}.

2.2. The High Altitude Auroral Acceleration Region

Returning to Figure 1, the sole assumption of the model is that the boundary condition imposed on the auroral acceleration region is an upward field-aligned current. As discussed in section 2.1, there is a density change across the lower boundary of the acceleration region such that the density above the lower boundary is low in the sense that the plasma must be accelerated to carry this imposed field-aligned current. (The shading in Figure 1 denotes the high density.)

The imposed field-aligned current density increases with decreasing altitude because of the converging magnetic field. Because electrons are also mirroring in this field, there may be an altitude below which the current density cannot be carried by the plasma existing at and below that altitude. This altitude is the upper border of the auroral acceleration region illustrated in Figure 1. Determining its location is one of the primary purposes of this paper. Knight [1973] was the first to consider parallel electric field acceleration caused by the effects of the converging magnetic field, and the results reported in this paper are consistent with this type of model. (For purposes of orientation, the high-, middle-, and low-altitude regions discussed below will be found to be roughly at 2.5-3 Earth radii, 2-2.5 Earth radii, and below ~2 Earth radii geocentric, respectively.)

This high-altitude upward parallel electric field drives electrons into the lower-altitude region. To have charge neutrality, positive charges must also be injected into this region. This is the function of the low-altitude, large-amplitude electric field whose physics is the same as that of sheaths in plasmas or the wall in a lab device, each of which produces an accelerating electric field in response to the requirement of charge neutrality in the neighboring region. A second benefit of this low-altitude parallel field is to exclude secondary electrons from the middle-altitude region.

The high- and low-altitude electric fields may not be enough to guarantee local charge neutrality without a distributed, parallel electric field through the middle-altitude region. Thus, in summary, three mechanisms that produce parallel electric fields in the auroral acceleration region result from imposing a field-aligned current in a low-density plasma.

Data from some 200 passes of Polar through the premidnight auroral zone have been examined to verify predictions of this model, to determine the high-altitude extent of the auroral acceleration region, and to estimate the amplitude of the parallel fields in the higher-altitude regions. These results will be discussed by first considering data acquired at altitudes above the auroral acceleration region and then, moving this discussion down in altitude, until parallel electric fields are encountered.

Plate 2 presents 40 min of data acquired at geocentric altitudes between 6.2 and 5.5 Earth radii. These data are typical of those studied during more than 50 Polar passes at similar altitudes in the spring and fall of 1996 and 1997. The panels in Plate 2 are the same as those previously discussed for Plate 1. During this time

interval and all others observed above ~2.5 Earth radii, the parallel electric field (Plate 2c) was less than the uncertainty in its measurement, which is typically less than 10% of the perpendicular field strength. The perpendicular field was turbulent and as large as 100 mV m^{-1} (Plates 2a and 2b), which would map to the ionosphere in the absence of lower altitude parallel fields to a magnitude in excess of a few mV m^{-1}. From the fact that such large fields are not observed in the ionosphere, there must have been a parallel field below the spacecraft from ~1020 to 1030 UT.

During this same time interval, an upgoing ion beam was observed with energies approaching 10 keV (Plate 2g). This ion data appears speckled because the beam was confined to small pitch angles and the Hydra detectors did not always sample this region of phase space. During the ion beam interval there were no signatures of acceleration in the electrons (plates 2i and 2j), as will be further discussed below. Because upgoing ions were observed in the absence of electron acceleration above the spacecraft, it is concluded that the spacecraft was both on magnetic field lines containing the auroral acceleration region and above all such parallel field acceleration.

The perpendicular potential crossed by the spacecraft (Plate 2e) was ~10 keV, which is consistent with the observed ion energy under the assumption that this perpendicular potential was converted to parallel potential below the spacecraft, as illustrated in the model of Figure 1.

The field-aligned current (Plate 2f) was upward and roughly constant from ~1020 to 1045 UT. However, the ion and electric field data indicate that there were parallel fields below the spacecraft only during the first 40% of this interval. So the question arises as to what happened near 1030 UT that allowed the current to flow after this time without requiring a parallel electric field below the spacecraft. An answer is that the plasma density above the acceleration region increased by a factor of more than 10 just after 1030 UT, so the field-aligned currents could be carried through the lower-altitude region without the need for a parallel electric field after this time. This density increase is evident in the spacecraft potential (Plate 2a) [*Scudder et al*., 2000] and in the electron distributions of Plates 2i and 2j. This explanation is supported by a quantitative estimate. The spacecraft potential of ~10 V after 1030 UT corresponds to a plasma density of ~1 particle cm^{-3}. An isotropic electron distribution with this density and an average energy of 1 keV contains enough particles in its ionospheric loss cone for electrons to carry the observed field-aligned current (that produced a slope in B_y of 1 nT min^{-1}) to the ionosphere along adiabatic trajectories without a parallel accelerating potential being required. On the other hand, the plasma density of ~0.3 particles cm^{-3} before 1030 UT is insufficient for carrying the same current to the ionosphere without imposition of a parallel potential.

The above discussion assumes that there was no parallel electric field above the spacecraft during the event of Plate 2. However, the electron data of Plates 2i and 2j might be consistent with a parallel potential as large as several kilovolts appearing above the spacecraft at and after 1030 UT, because such a potential changes the intensity of a Maxwellian distribution, above a low-energy cutoff, without changing its spectral shape. That this explanation does not fit the observed spectra is illustrated in Fig. 3, which gives down-going electron distribution functions before and after the change near 1030 UT. Because this change was a temperature

increase of a Maxwellian distribution, the spectrum after this time cannot be obtained by passing the spectrum obtained before this time through a parallel potential. Thus parallel fields do not cause the density and temperature increases around 1030 UT. Instead, such increases must be associated with a change in the plasma source. This type of spectrum in the differential energy flux was observed generally in the many Polar passes studied in this altitude range, and variations of intensity and temperature such as those in Plate 2 are also common features of this data.

High-altitude electron data cannot rule out that the plasma sheet electrons were accelerated through potentials that are small compared to the electron temperature of several kilovolts, because such parallel potentials are difficult to measure in terms of their effects on the electron spectra. (It might be argued that a low-energy cutoff in the down-going electron energy spectrum would be produced by acceleration above the spacecraft. Such a cutoff is not seen. This result could be explained as due to filling of the gap in the low-energy spectrum by any number of processes.) However, in the particular case of Plate 2, such small parallel potentials were not present, at least after 1035 UT. Evidence for this conclusion is associated with the low-energy fluxes of counterstreaming electrons observed between ~1038 and 1045 UT. The distribution function of these electrons is presented in Plate 3. While the origin of these electrons is beyond the scope of this work, examination of upgoing and downgoing fluxes at velocities above ~5000 km s^{-1} shows that the upward going electrons were not reflected by a potential above the spacecraft to reappear at the spacecraft as downward going electrons. Thus the potential above the spacecraft must have been less than that required to reflect electrons with velocities of ~5000 km s^{-1} or energies of ~70 eV. Such counter-streaming electrons are relatively common in the data.

Because the parallel potential above the spacecraft is not discernable when it is small compared to the electron temperature, possible parallel potentials of a few hundred volts are neglected in defining the top of the auroral acceleration region in this study. It should be pointed out that such potentials may well exist on auroral field lines at higher altitudes because they may be required to move otherwise-mirroring electrons to lower altitudes where the major parallel potential exists (R. E. Ergun, private communication, 2000).

The discussion of fields and particles at geocentric altitudes of 6 Earth radii will be completed by considering the example of Plate 4. In these data, the upward field-aligned current intensity (Plate 4f) near 0954 UT was about as large as that generally observed at these altitudes, producing a slope in B_y of ~20 nT min^{-1}. The large, turbulent electric field and the upgoing ions show the existence of a parallel potential below the spacecraft at this time, when the local plasma density was ~2 particles cm^{-3} (Plate 4d). For an isotropic electron distribution having this density and an average energy of a few hundred volts (Plates 4i and 4j), the electrons in the ionospheric loss cone were unable to carry the large field-aligned current by about an order-of-magnitude, so a parallel potential was required. However, between ~0957 and 1003 UT the field aligned current was an order of magnitude smaller, and the density was more than a factor of 2 greater, so no parallel potential below the spacecraft should be expected, and none was observed in either the electric field or upgoing ions.

An example of plasma and field data at altitudes of 4.0 to 4.7 geocentric Earth radii is given in Plate 5. These data also show

that the spacecraft was on magnetic field lines above a parallel electric field region, because there are upgoing ion beams (Plate 5g) and large, turbulent, perpendicular electric fields that would map to the ionosphere as fields of ~V m^{-1} in the absence of parallel fields below the spacecraft (Plates 5a and 5b). There was no measurable parallel electric field component (third panel). The upward flowing ions were observed in each of two upward field-aligned current regions (Plate 5f, where an upward current is associated with a positive slope), and their energy is greater in the current region having the lower density (Plate 5d). This is further evidence that the plasma density controls the existence and size of the parallel electric fields. The ion distribution function measured near 0233 UT is given in Plate 6. The upward ion beam is clearly separated from the core distribution, which is evidence for parallel field acceleration.

Across the change in field-aligned current direction near 0224 UT in Plate 5, the several keV electron distribution did not change. This is proof that the peaked differential energy flux distribution of these plasma sheet electrons is not the consequence of a parallel electric field above the spacecraft in the upward field-aligned current region.

Plate 7 presents 13 min of Polar data as the spacecraft moved from a geocentric altitude of 3.5 to 3.1 Earth radii. The perpendicular electric field approached 80 mV m^{-1} and the parallel field was consistent with zero (Plate 7a-7c). Because this perpendicular field would map to the ionosphere as a large fraction of one V m^{-1} in the absence of parallel fields below the spacecraft, such parallel fields must have existed. Upgoing ions were observed from ~2346 to 2353 UT, and their peak energy of ~3 keV was consistent with the perpendicular potential encountered by the spacecraft and available as a parallel potential below the spacecraft (Plate 7e).

The field-aligned current in Plate 7 was upward from ~2346 to 2356 UT, and it was roughly constant except for two brief periods (Plate 7f, where an upward current is associated with a negative slope). During the last 4 min of this interval, there were no parallel fields below the spacecraft because there were no upgoing ion beams or large perpendicular electric fields. The presence of parallel fields below the spacecraft before 2352 UT, and not afterwards, can be explained by the increase of plasma density by more than a factor of 10 between 2350 and 2352 UT (Plate 7d). The Hydra electrons also showed a similar density increase at this time. Thus these data are also consistent with the model that parallel electric fields arise when the plasma density is insufficient to carry the imposed field-aligned current.

In the case of Plate 7, it is more difficult to decide whether there was a parallel potential above the spacecraft and what its magnitude may have been. The increased electron intensity for a minute around 2347 UT is not consistent with the distribution before or after that time having passed through a parallel potential above the spacecraft. There may have been a parallel potential above the spacecraft near an altitude of 3.3 Earth radii near 2354 UT, because of the inverted-V shape of the electron distribution (although this feature sometimes occurs at higher altitudes, where it is not likely that significant parallel electric fields exist above the spacecraft). This potential could have been as large as 1 kV. Thus the first signs of a significant parallel potential above the spacecraft may have appeared at a geocentric altitude somewhat above 3 Earth radii.

An example of data below 3 Earth radii is given in Plate 8. As

the spacecraft rose from 2.7 to 3.2 Earth radii during the 20-min interval of Plate 8, it encountered two upgoing ion beam events (Plate 8d). The energy of these ions increased from below 1 keV in the first event to ~8 keV in the second event. This energy increase is consistent with a constant upward parallel electric field of ~3 mV m^{-1} between 2.7 and 3.0 Earth radii, under the assumption that the energy change was due to an altitude dependence and not to a time or latitude dependence. A well-defined inverted-V electron distribution was measured in the first event with peak energy of ~5 keV (Plates 8i and 8j). In the second event there was no evidence for electron acceleration above the spacecraft after an inverted-V signature was observed before 1700 UT. The electron results are also consistent with a parallel electric field of a few mV m^{-1} between 2.7 and 3.0 Earth radii.

The upward field-aligned current (positive slope in Plate 8f) in the first event was an order of magnitude larger than that in the second event. This result is consistent with equal magnitudes of the parallel potentials associated with both events, when consideration is given to the fact that the plasma density was higher in the first event by at least an order of magnitude (Plate 8d).

The data of Plate 9, at geocentric altitudes between 2.4 and 3.2 Earth radii, provide another example of the upper altitude limit of the auroral acceleration region. The perpendicular electric field was larger than 200 mV m^{-1} and the average (nonwave) parallel electric field was small. As the spacecraft rose in altitude, it passed through three regions of upward ion beams (Plate 9g). The first, centered near 1648 UT, was accompanied by a well-defined electron inverted-V event (Plates 9i and 9j). The electron energies were as great as 7 keV and they exceeded the ion beam energy by at least a factor of 2, showing that the spacecraft was deep in the acceleration region at an altitude of 2.4 Earth radii. In each succeeding ion event, near 1703 and 1706 UT, respectively, the ion energy increased, as if the spacecraft passed through a parallel potential of ~7 kV in rising to 3 Earth radii. Similarly, signatures of inverted-V electrons in the second and third ion events were lacking, indicating again that the spacecraft had moved above a substantial part of the 7 kV potential through which the electrons in the first ion event had been accelerated. Thus the ion and electron data of Plate 9 are explained by the upper end of the acceleration region being at ~3 Earth radii and that a 7-kV potential existed between 2.4 and 3.1 Earth radii. The average electric field associated with this potential is ~1.5 mV m^{-1}.

In Figure 4, a scatterplot of the ion energy divided by the sum of the ion and electron energies in ~40 upgoing ion events having a total parallel potential in excess of 1 kV, is plotted as a function of geocentric altitude. The ordinate in Figure 4 is equal to the fraction of the parallel potential below the satellite. Values of this ratio greater than ~0.8 are consistent with essentially all of the potential (other than a possible few hundred volts) being below the spacecraft because it is difficult to discern an acceleration potential of hundreds of volts in a spectrum of 10 keV plasma sheet electrons. For this reason the data of Figure 4 were obtained by hand analysis, and not by a computer program. From this figure, it is seen that the upper end of the auroral acceleration is at a geocentric altitude of 3-3.5 Earth radii at local times of 2000-2400 UT during the spring or autumnal equinoxes. Since about half of the typically 5 kV parallel potential exists between altitudes of 2.5 and 3.0 Earth radii, the average parallel electric field in this region is ~2.0 mV m^{-1}.

3. Summary

In summary, the following points are made in this paper:

1. Parallel electric potentials greater than a few hundred volts in the upward current portion of the auroral acceleration region extend upward to geocentric altitudes of 3.0-3.5 Earth radii.

2. The three mechanisms that produce parallel fields in the presence of an imposed field-aligned current are associated with (1) the high-altitude field required to accelerate downgoing electrons in order that they can carry the imposed field-aligned current, (2) the low-altitude sheath field required to maintain gross charge neutrality by injecting ions into the midaltitude region and preventing backscattered electrons from reaching this region, and (3) the midaltitude field required to guarantee local charge neutrality.

3. The parallel, low-altitude sheath field can be as large as several hundred mV m^{-1}, while the higher-altitude parallel fields have magnitudes of a few mV m^{-1}.

4. To produce parallel electric fields and discrete auroras in the auroral acceleration region, all that is needed is an imposed, uniform, upward field-aligned current and a decreased density, such that particle acceleration is required to carry the imposed current.

These results are consistent with the idea first advanced by *Knight* [1973] and expanded by *Chiu and Schulz* [1978] and *Lyons* [1980] that the field-aligned potential arises when the plasma is insufficient to carry the imposed field-aligned current through the converging magnetic field. Although these theories produce a field-aligned potential that is a function of both the current density and the plasma density, the current density has assumed the more important role in current disruption models of substorms that are triggered by an abrupt increase of the field-aligned current. The present work suggests that the plasma density may play a more significant role in substorm physics than has been thought previously. The theories of Knight, Chiu and Schulz, and Lyons predict the magnitude of the potential drop but not the location or size of the parallel electric field. Recently R. E. Ergun et al. (Parallel electric fields in discrete arcs, submitted to Journal of Geophysical Research, 2000) have proposed a model that invokes only what amounts to charge neutrality and that yields the electric field as a function of altitude. This model produces results in general agreement with the experimental data that are presented in this paper.

Acknowledgments. The authors thank C. W. Carlson, R. Ergun, J. P. McFadden, and M. Temerin for many helpful discussions and ideas. They also thank the HYDRA and Magnetic Field Instrument teams and specifically P.I.s Jack Scudder and Chris Russell, for providing excellent instruments and allowing free use of their data. This work was supported by NASA grants NAG5-3182 and 19982924.

Hiroshi Matsumoto thanks T. Yamamoto and G. Maerendel for their assistance in evaluating this paper.

References

Chiu,Y.T., and M. Schulz, Self-consistent particle and parallel electrostatic field distributions in the magnetospheric-ionospheric auroral region, *J. Geophys. Res.*, ***83***, 629, 1978.

Evans, D.S., Precipitation electron fluxes formed by a magnetic field-aligned potential difference, *J. Geophys. Res*., *79*, 2853, 1974.

Haerendel, G., et al., First observation of electrostatic acceleration of barium ions into the magnetosphere, *Euro Space Agency Spec. Publ*.-155, 203, 1976.

Harvey, P.R., et al., The electric field instrument on the Polar satellite, *Space Sci. Rev*., *71*, 583, 1995.

Knight, L., Parallel electric fields, *Planet. Space Sci.*, *21*, 741, 1973.

Lyons, L.R., Generation of large-scale regions of auroral currents, electric potentials, and precipitation by the divergence of the convection electric field, *J. Geophys. Res*., *85*, 17, 1980.

McFadden, J.P., C. W. Carlson, and R.E. Ergun, Microstructure of the auroral acceleration region as observed by FAST, *J. Geophys. Res*., *104*, 14,453, 1999.

McIlwain, C.E., Direct measurement of particles producing visible auroras, *J. Geophys. Res*., *65*, 2727, 1960.

Mozer, F.S., et al., Observations of paired electrostatic shocks in the polar magnetosphere, *Phys. Rev. Lett.*, *38*, 292, 1977.

Mozer, F.S., et al., Satellite measurements and theories of low altitude auroral particle acceleration, *Space Sci. Rev*., *27*, 155, 1980.

Mozer, F.S., and C.A. Kletzing, Direct observation of large, quasi-static, parallel electric fields in the auroral acceleration region, *Geophys. Res. Lett.*, *25*, 1629, 1998.

Russell, C.T., et al., The GGS/Polar Magnetic Fields Investigation, *Space Sci. Rev.*, *71*, 563, 1995.

Scudder, J. et al, Hydra: A three dimensional electron and ion hot plasma instrument for the Polar spacecraft of the GGS mission, *Space Sci. Rev*., *71*, 459, 1995.

Scudder, J.D., X. Cao, and F.S. Mozer, Photoemission current-spacecraft voltage relation: Key to routine, quantitative low-energy plasma measurements, *J. Geophys. Res.*, *105*, 21281, 2000

Shelley, E.G., et al., Satellite observations of an ionospheric acceleration mechanism, *Geophys. Res. Lett.*, *3*, 654, 1976.

A. Hull and F. S. Mozer, Space Sciences Laboratory, University of California, Berkeley, CA 94720-7450. (mozer@sunspot.ssl.berkeley.edu)

(Received April 25, 2000; revised July 4, 2000;
accepted August 9, 2000.)

Paper number 2000JA900117.
0148-0227/00/2000JA900117$09.00

Figure 1. Model of electric equipotentials in a meridional plane, between the ionosphere and the magnetosphere, in which magnetic field lines are vertical.

Figure 2. (a-d) Raw electric field, spacecraft potential, and westward magnetic field measured in the Southern Hemisphere on May 3, 1997, during an interval containing three potential fingers.

Figure 3. Electron energy spectra obtained before and after the intensity change that occurred near 1030 UT on May 16, 1996.

Figure 4. The fraction of the parallel potential below the Polar geocentric altitude, as a function of altitude.

Plate 1. (a-j) Fields and particles observed in the Southern Hemisphere on May 8, 1999, at a magnetic local time near 2125.

Plate 2. (a-j) Fields and particles observed in the Northern Hemisphere on May 16, 1996, at a magnetic local time near 2130.

Plate 3. The low-energy electron distribution function on May 16, 1996, during the observation of counterstreaming low-energy electrons.

Plate 4. (a-j) Fields and particles observed in the Northern Hemisphere on April 8, 1996, at a magnetic local time near midnight.

Plate 5. (a-j) Fields and particles observed in the Northern Hemisphere on November 28, 1996, at a magnetic local time near 2120.

Plate 6. The ion distribution function measured during the event of November 28, 1996.

Plate 7. (a-j) Fields and particles observed in the Northern Hemisphere on April 11, 1999, at a magnetic local time near 0000.

Plate 8. (a-j) Observations in the Southern Hemisphere on October 13, 1999, at a magnetic local time near 2300. The spinperiod averaged electric field components are illustrated. The small, apparently nonzero, parallel electric fields observed near 1653 and 1700 UT are due to the rectification of high-frequency waves and are not an indication of a large parallel DC field. The discontinuity in the magnetic field near 1704 UT is due to a mode change in the instrument.

Plate 9. (a-j) Fields and particles observed in the Southern Hemisphere on November 9, 1999, at a magnetic local time near 2030.

Figure 1. Model of electric equipotentials in a meridional plane, between the ionosphere and the magnetosphere, in which magnetic field lines are vertical.

Figure 2. (a-d) Raw electric field, spacecraft potential, and westward magnetic field measured in the Southern Hemisphere on May 3, 1997, during an interval containing three potential fingers.

Figure 3. Electron energy spectra obtained before and after the intensity change that occurred near 1030 UT on May 16, 1996.

Figure 4. The fraction of the parallel potential below the Polar geocentric altitude, as a function of altitude.

Plate 1. (a-j) Fields and particles observed in the Southern Hemisphere on May 8, 1999, at a magnetic local time near 2125.

Plate 2. (a-j) Fields and particles observed in the Northern Hemisphere on May 16, 1996, at a magnetic local time near 2130.

Plate 3. The low-energy electron distribution function on May 16, 1996, during the observation of counterstreaming low-energy electrons.

Plate 4. (a-j) Fields and particles observed in the Northern Hemisphere on April 8, 1996, at a magnetic local time near midnight.

Plate 5. (a-j) Fields and particles observed in the Northern Hemisphere on November 28, 1996, at a magnetic local time near 2120.

Plate 6. The ion distribution function measured during the event of November 28, 1996.

Plate 7. (a-j) Fields and particles observed in the Northern Hemisphere on April 11, 1999, at a magnetic local time near 0000.

Plate 8. (a-j) Observations in the Southern Hemisphere on October 13, 1999, at a magnetic local time near 2300. The spinperiod averaged electric field components are illustrated. The small, apparently nonzero, parallel electric fields observed near 1653 and 1700 UT are due to the rectification of high-frequency waves and are not an indication of a large parallel DC field. The discontinuity in the magnetic field near 1704 UT is due to a mode change in the instrument.

Plate 9. (a-j) Fields and particles observed in the Southern Hemisphere on November 9, 1999, at a magnetic local time near 2030.

MOZER AND HULL: ORIGIN AND GEOMETRY OF UPWARD PARALLEL ELECTRIC FIELDS

MOZER AND HULL: ORIGIN AND GEOMETRY OF UPWARD PARALLEL ELECTRIC FIELDS

MOZER AND HULL: ORIGIN AND GEOMETRY OF UPWARD PARALLEL ELECTRIC FIELDS

MOZER AND HULL: ORIGIN AND GEOMETRY OF UPWARD PARALLEL ELECTRIC FIELDS

MOZER AND HULL: ORIGIN AND GEOMETRY OF UPWARD PARALLEL ELECTRIC FIELDS

MOZER AND HULL: ORIGIN AND GEOMETRY OF UPWARD PARALLEL ELECTRIC FIELDS

MOZER AND HULL: ORIGIN AND GEOMETRY OF UPWARD PARALLEL ELECTRIC FIELDS

MOZER AND HULL: ORIGIN AND GEOMETRY OF UPWARD PARALLEL ELECTRIC FIELDS

MOZER AND HULL: ORIGIN AND GEOMETRY OF UPWARD PARALLEL ELECTRIC FIELDS

MOZER AND HULL: ORIGIN AND GEOMETRY OF UPWARD PARALLEL ELECTRIC FIELDS

MOZER AND HULL: ORIGIN AND GEOMETRY OF UPWARD PARALLEL ELECTRIC FIELDS

MOZER AND HULL: ORIGIN AND GEOMETRY OF UPWARD PARALLEL ELECTRIC FIELDS

MOZER AND HULL: ORIGIN AND GEOMETRY OF UPWARD PARALLEL ELECTRIC FIELDS

MOZER AND HULL: ORIGIN AND GEOMETRY OF UPWARD PARALLEL ELECTRIC FIELDS

MOZER AND HULL: ORIGIN AND GEOMETRY OF UPWARD PARALLEL ELECTRIC FIELDS

MOZER AND HULL: ORIGIN AND GEOMETRY OF UPWARD PARALLEL ELECTRIC FIELDS

MOZER AND HULL: ORIGIN AND GEOMETRY OF UPWARD PARALLEL ELECTRIC FIELDS

MOZER AND HULL: ORIGIN AND GEOMETRY OF UPWARD PARALLEL ELECTRIC FIELDS

MOZER AND HULL: ORIGIN AND GEOMETRY OF UPWARD PARALLEL ELECTRIC FIELDS

MOZER AND HULL: ORIGIN AND GEOMETRY OF UPWARD PARALLEL ELECTRIC FIELDS

MOZER AND HULL: ORIGIN AND GEOMETRY OF UPWARD PARALLEL ELECTRIC FIELDS

MOZER AND HULL: ORIGIN AND GEOMETRY OF UPWARD PARALLEL ELECTRIC FIELDS

MOZER AND HULL: ORIGIN AND GEOMETRY OF UPWARD PARALLEL ELECTRIC FIELDS

MOZER AND HULL: ORIGIN AND GEOMETRY OF UPWARD PARALLEL ELECTRIC FIELDS

MOZER AND HULL: ORIGIN AND GEOMETRY OF UPWARD PARALLEL ELECTRIC FIELDS

MOZER AND HULL: ORIGIN AND GEOMETRY OF UPWARD PARALLEL ELECTRIC FIELDS

MOZER AND HULL: ORIGIN AND GEOMETRY OF UPWARD PARALLEL ELECTRIC FIELDS

MOZER AND HULL: ORIGIN AND GEOMETRY OF UPWARD PARALLEL ELECTRIC FIELDS

MOZER AND HULL: ORIGIN AND GEOMETRY OF UPWARD PARALLEL ELECTRIC FIELDS

MOZER AND HULL: ORIGIN AND GEOMETRY OF UPWARD PARALLEL ELECTRIC FIELDS

2000JA90017

Electric fields, magnetic fields, and plasmas measured on the Polar satellite are studied to determine the altitude extent of the upward field-aligned current portion of the auroral acceleration region and the physical processes that populate it with parallel electric fields. This region extends upward to a geocentric altitude of 3 or 3.5 Earth radii at premidnight local times during the spring and fall. In a model for this region a necessary but not sufficient condition for the appearance of parallel electric fields is an upward field-aligned current. Parallel electric fields will exist where the plasma density is insufficient to carry this imposed field-aligned current through the converging magnetic field. These parallel fields are associated with (1) high-altitude electron acceleration required to carry the imposed current through the low-density region; (2) a low-altitude sheath required to inject compensating positive charge into the region and to restrict entry of secondary electrons from below; and (3) the midaltitude maintenance of local charge neutrality. The parallel electric field in the low-altitude sheath is directly measured to be as large as several hundred mV m^{-1}, while the higher-altitude fields appear to have magnitudes of a few mV m^{-1}. The low-altitude sheath is corrugated in a manner that does not depend on striations of the field-aligned current but that may depend on density variations.

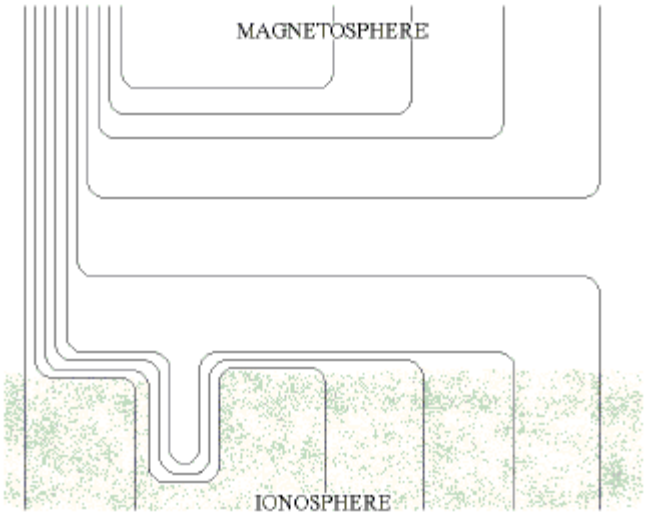

Figure 1

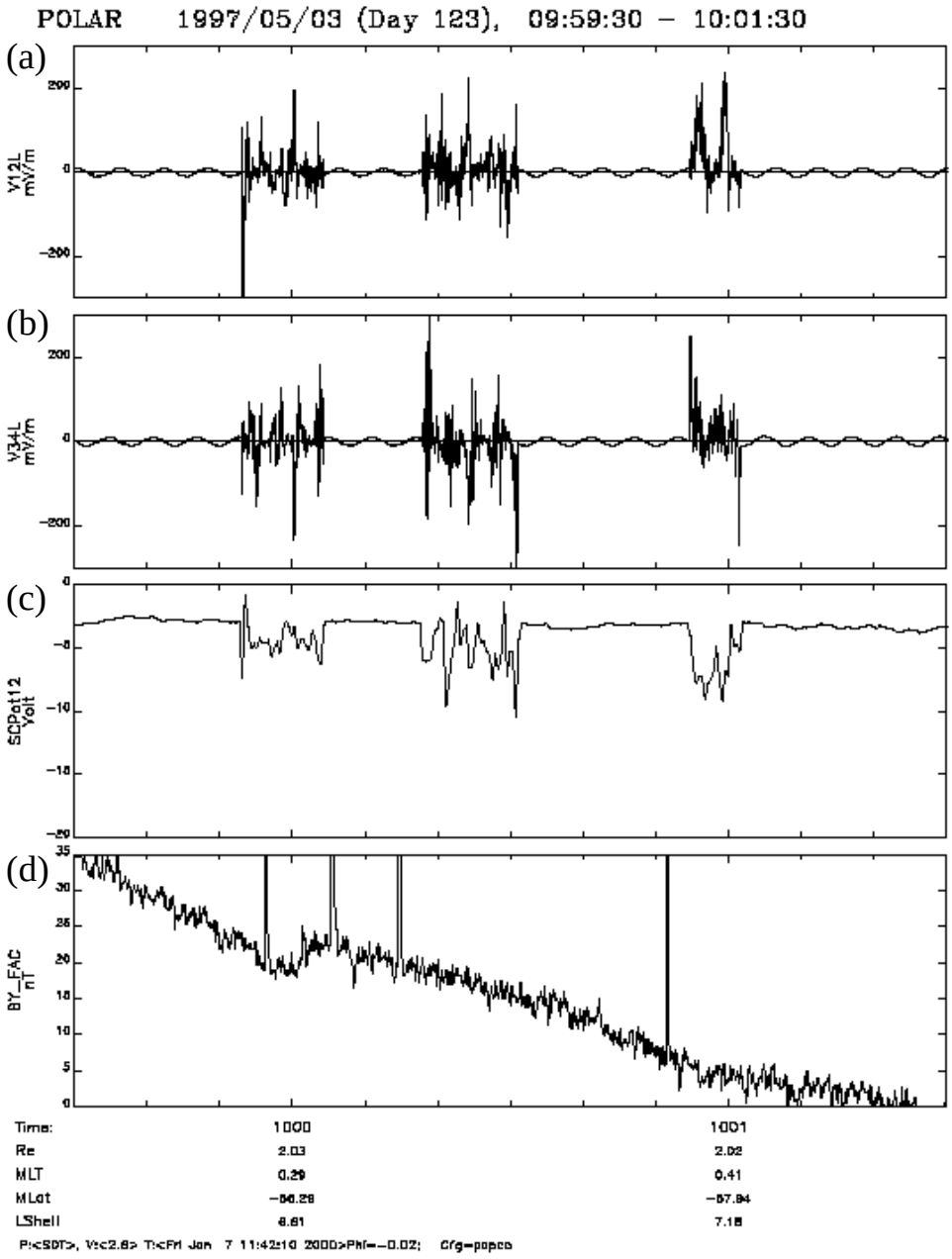
POLAR 1997/05/03 (Day 123), 09:59:30 – 10:01:30
(a)
V12L mV/m
200
0
−200
(b)
V34L mV/m
200
0
−200
(c)
SCPot12 Volt
0
−5
−10
−15
−20
(d)
BY_FAC nT
35
30
25
20
15
10
5
0
Time: 1000 1001
Re 2.03 2.02
MLT 0.29 0.41
MLat −56.28 −57.94
LShell 6.61 7.18
P:<SDT>, V:<2.6> T:<Fri Jan 7 11:42:10 2000>Phi=−0.02; Org=popco

Figure 2

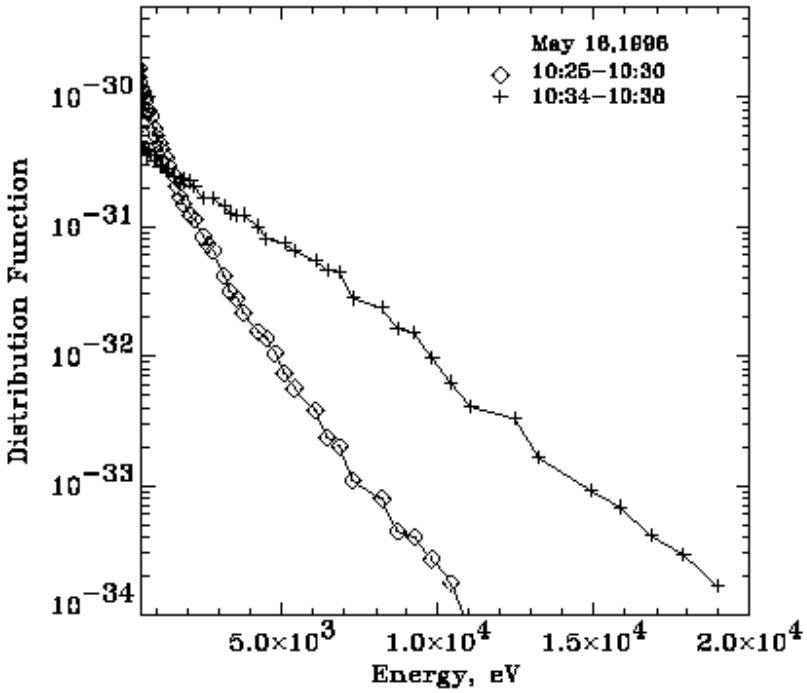
May 16,1996
10:25–10:30
10:34–10:38
Distribution Function
10^{-30}
10^{-31}
10^{-32}
10^{-33}
10^{-34}
5.0×10^{3}
1.0×10^{4}
1.5×10^{4}
2.0×10^{4}
Energy, eV

Figure 3

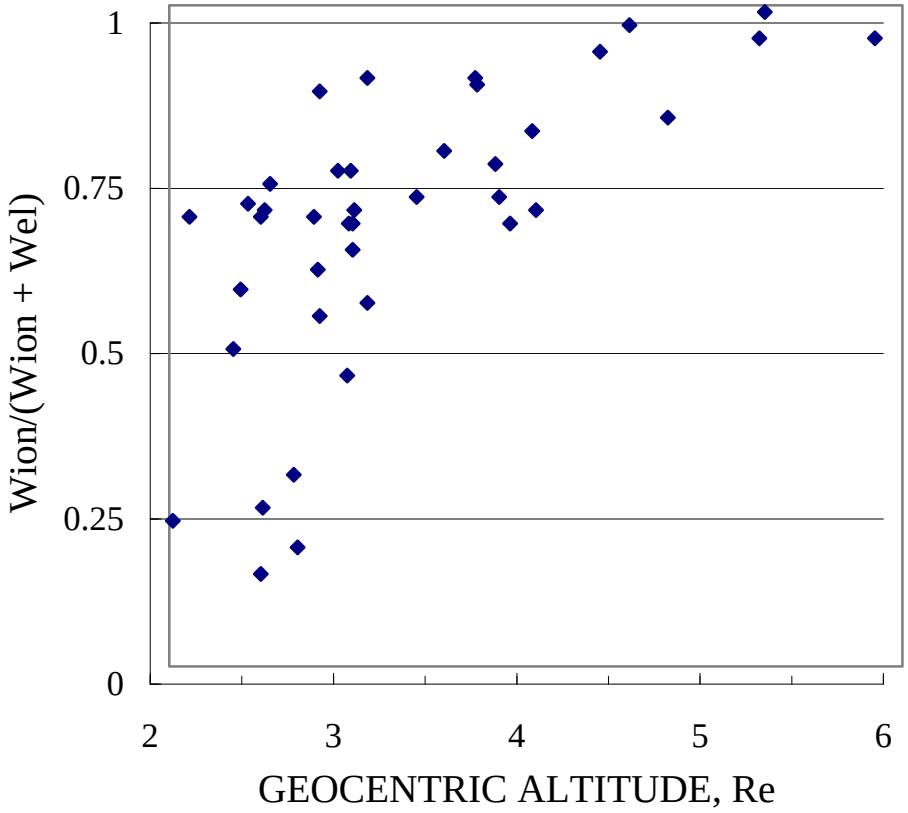

Figure 4

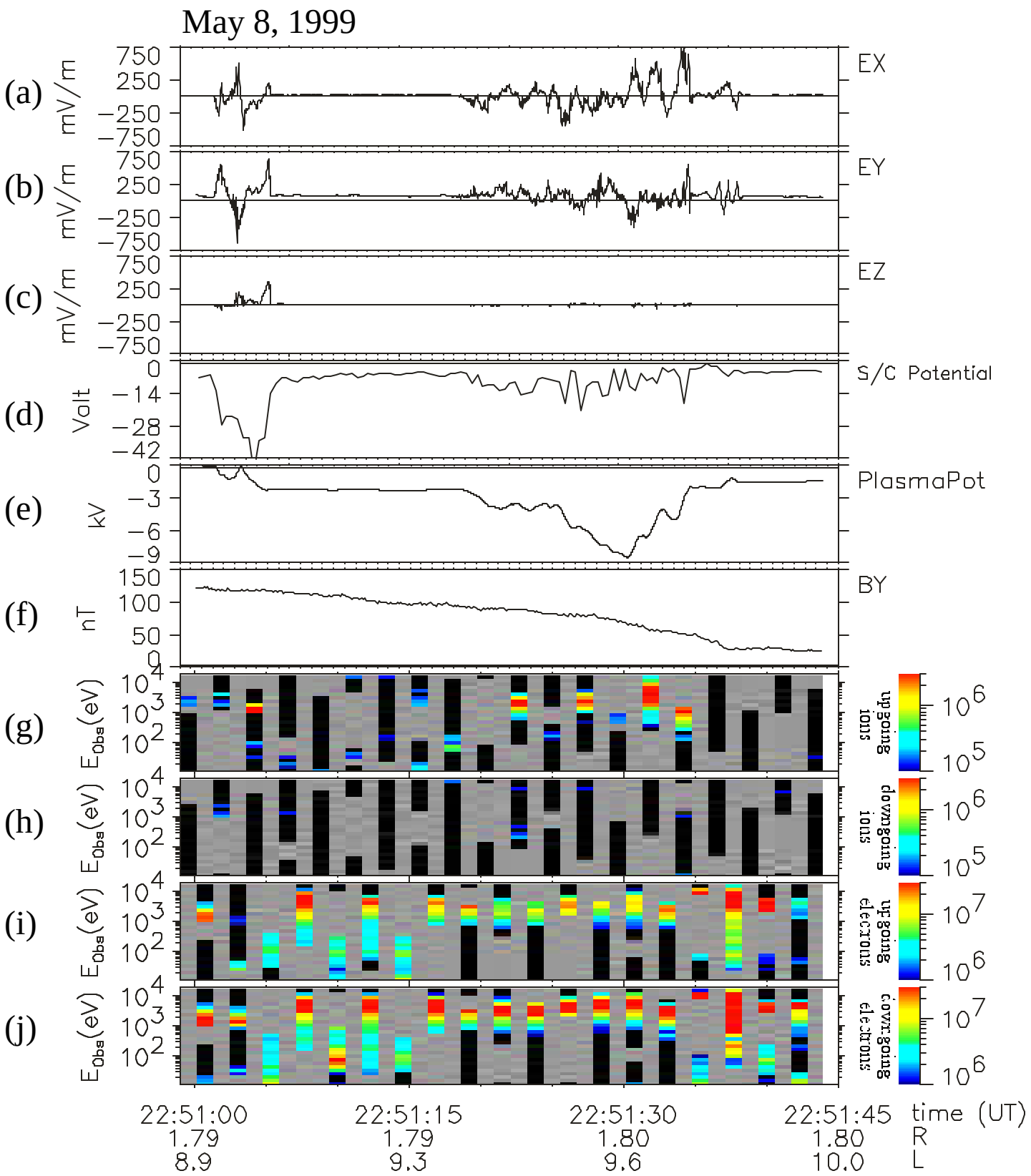
May 8, 1999
(a)
mV/m
750
250
−250
−750
EX
(b)
mV/m
750
250
−250
−750
EY
(c)
mV/m
750
250
−250
−750
EZ
(d)
Volt
0
−14
−28
−42
S/C Potential
(e)
kV
0
−3
−6
−9
PlasmaPot
(f)
nT
150
100
50
0
BY
(g)
E_Obs(eV)
10^4
10^3
10^2
upgoing ions
10^6
10^5
(h)
E_Obs(eV)
10^4
10^3
10^2
downgoing ions
10^6
10^5
(i)
E_Obs(eV)
10^4
10^3
10^2
upgoing electrons
10^7
10^6
(j)
E_Obs(eV)
10^4
10^3
10^2
downgoing electrons
10^7
10^6
22:51:00
1.79
8.9
22:51:15
1.79
9.3
22:51:30
1.80
9.6
22:51:45
1.80
10.0
time (UT)
R
L

Plate 1

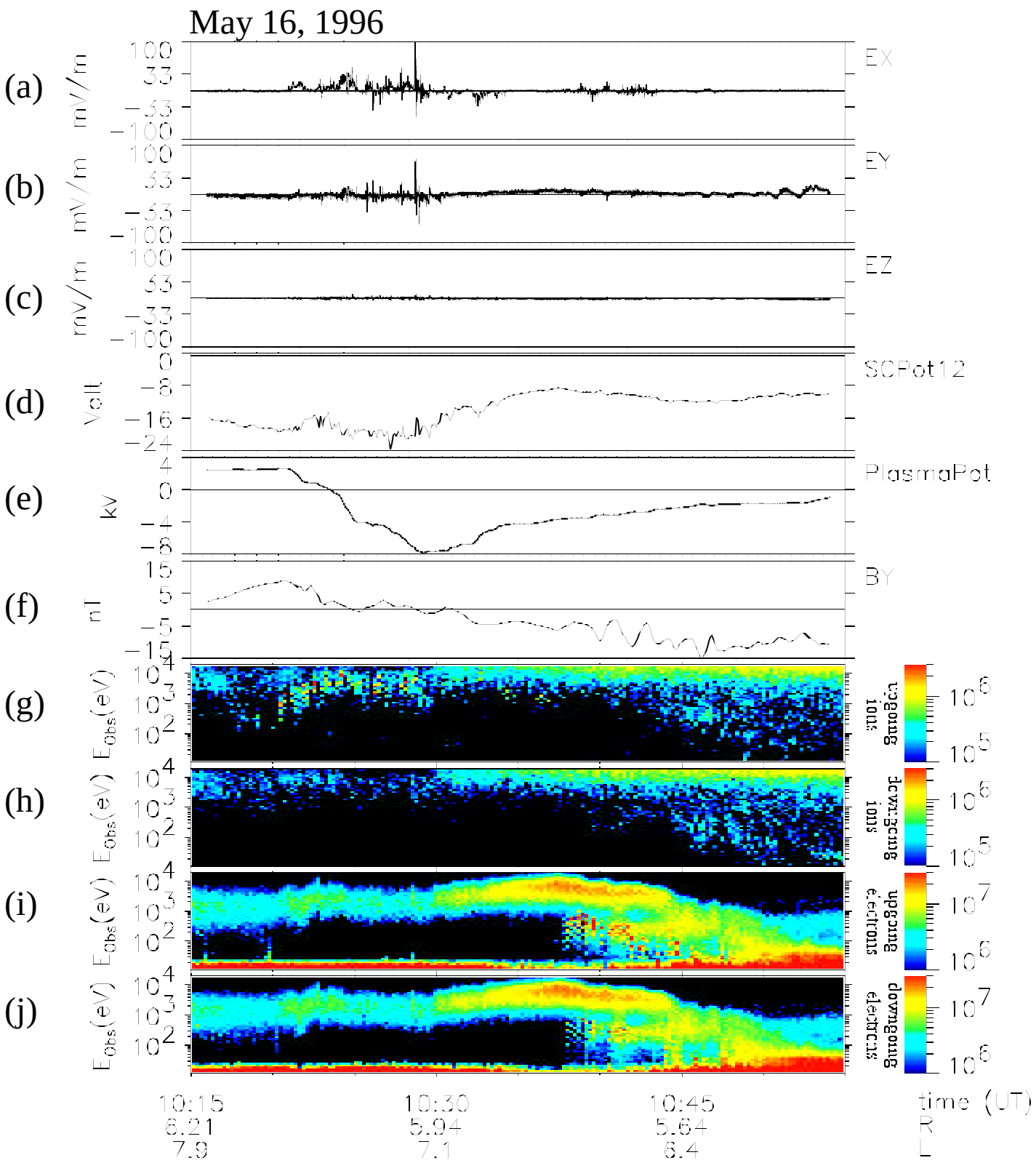
May 16, 1996
(a)
(b)
(c)
(d)
(e)
(f)
(g)
(h)
(i)
(j)
EX
EY
EZ
SCPot12
PlasmaPot
BY
mV/m
Volt
kV
nT
E_{Obs}(eV)
upgoing ions
downgoing ions
upgoing electrons
downgoing electrons
10:15
6.21
7.9
10:30
5.94
7.1
10:45
5.64
6.4
time (UT)
R
L

Plate 2

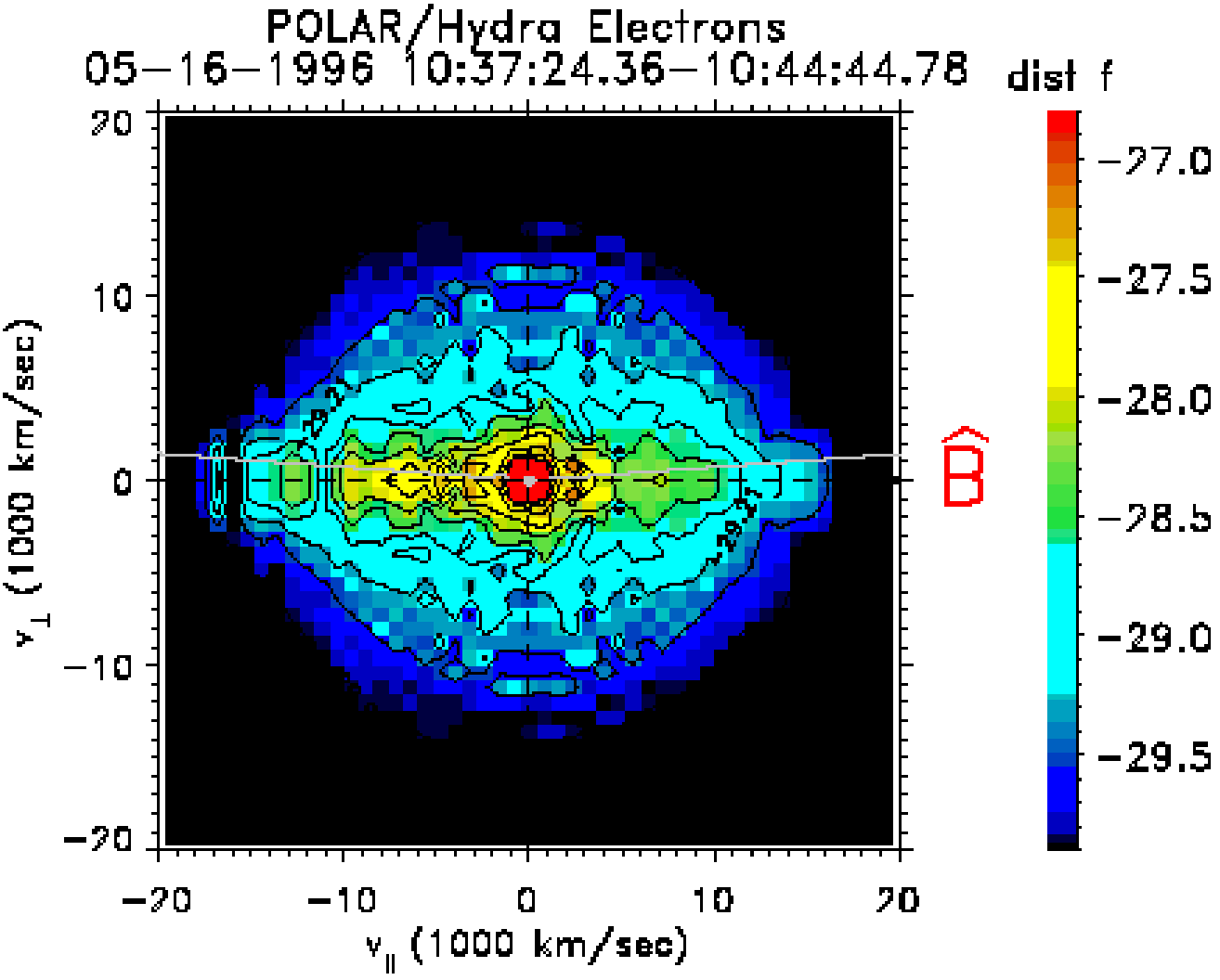
POLAR/Hydra Electrons
05–16–1996 10:37:24.36–10:44:44.78
dist f
-27.0
-27.5
-28.0
-28.5
-29.0
-29.5
B
20
10
0
−10
−20
−20
−10
0
10
20
v⊥ (1000 km/sec)
v|| (1000 km/sec)

Plate 3

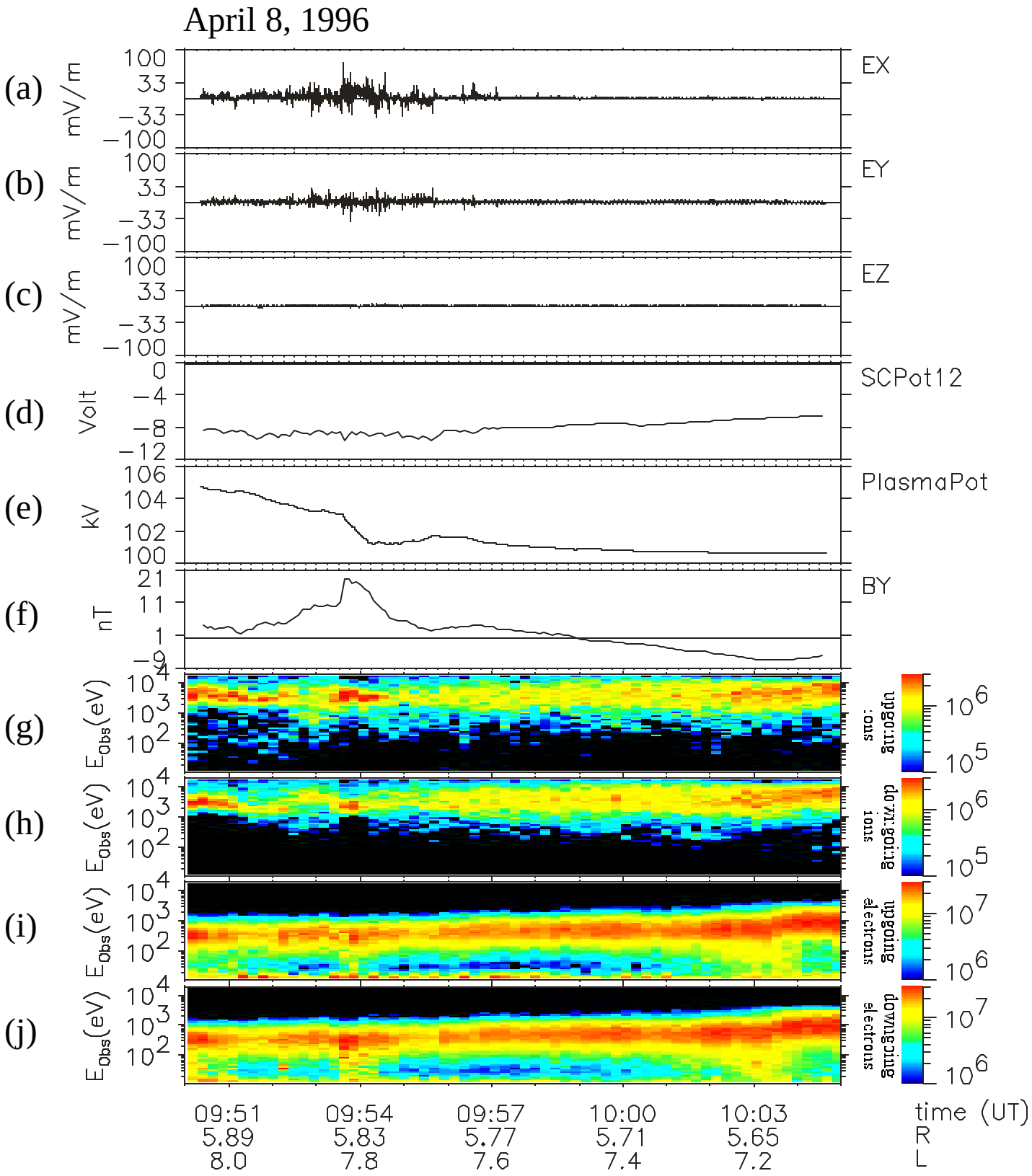
April 8, 1996
(a)
(b)
(c)
(d)
(e)
(f)
(g)
(h)
(i)
(j)
mV/m
Volt
kV
nT
EX
EY
EZ
SCPot12
PlasmaPot
BY
E_{Obs}(eV)
upgoing ions
downgoing ions
upgoing electrons
downgoing electrons
09:51
5.89
8.0
09:54
5.83
7.8
09:57
5.77
7.6
10:00
5.71
7.4
10:03
5.65
7.2
time (UT)
R
L

Plate 4

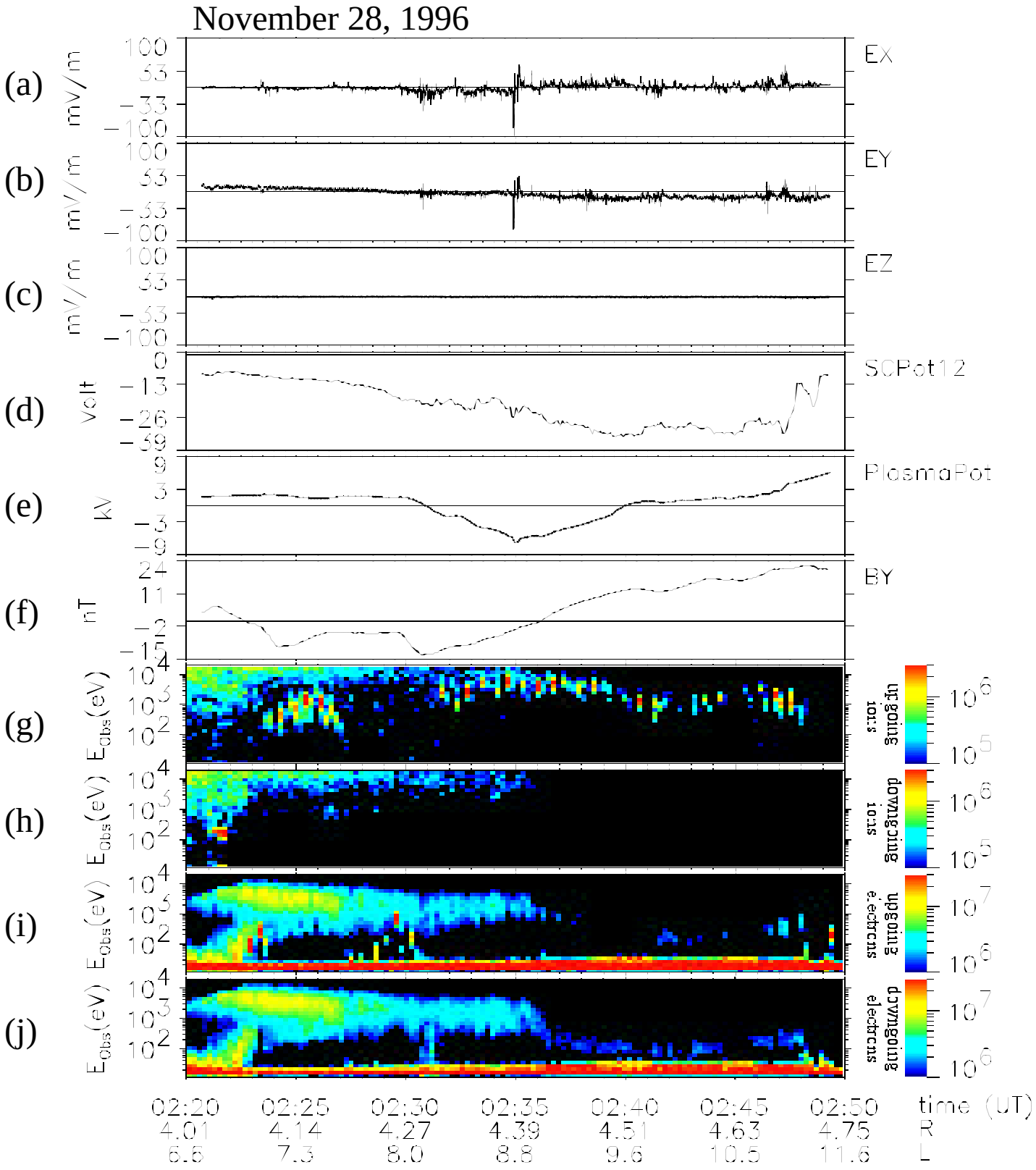
November 28, 1996
(a)
(b)
(c)
(d)
(e)
(f)
(g)
(h)
(i)
(j)
mV/m
EX
EY
EZ
volt
SCPot12
kV
PlasmaPot
nT
BY
E_Obs(eV)
upgoing ions
downgoing ions
upgoing electrons
downgoing electrons
02:20
02:25
02:30
02:35
02:40
02:45
02:50
time (UT)
4.01
4.14
4.27
4.39
4.51
4.63
4.75
R
6.6
7.3
8.0
8.8
9.6
10.5
11.6
L

Plate 5

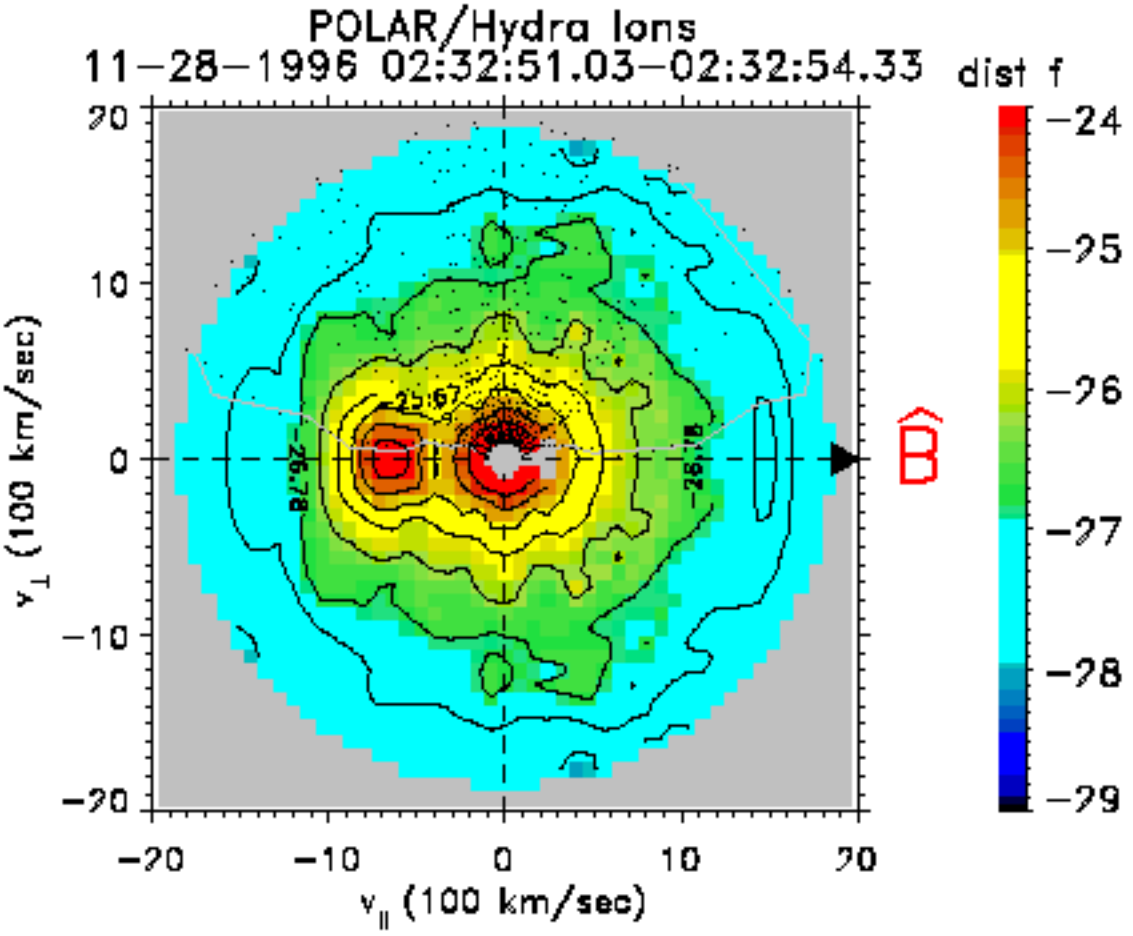
POLAR/Hydra Ions
11–28–1996 02:32:51.03–02:32:54.33
dist f
–24
–25
–26
–27
–28
–29
20
10
0
–10
–20
–20
–10
0
10
20
v⊥ (100 km/sec)
v|| (100 km/sec)
B
–25.67
–26.78
–26.78

Plate 6

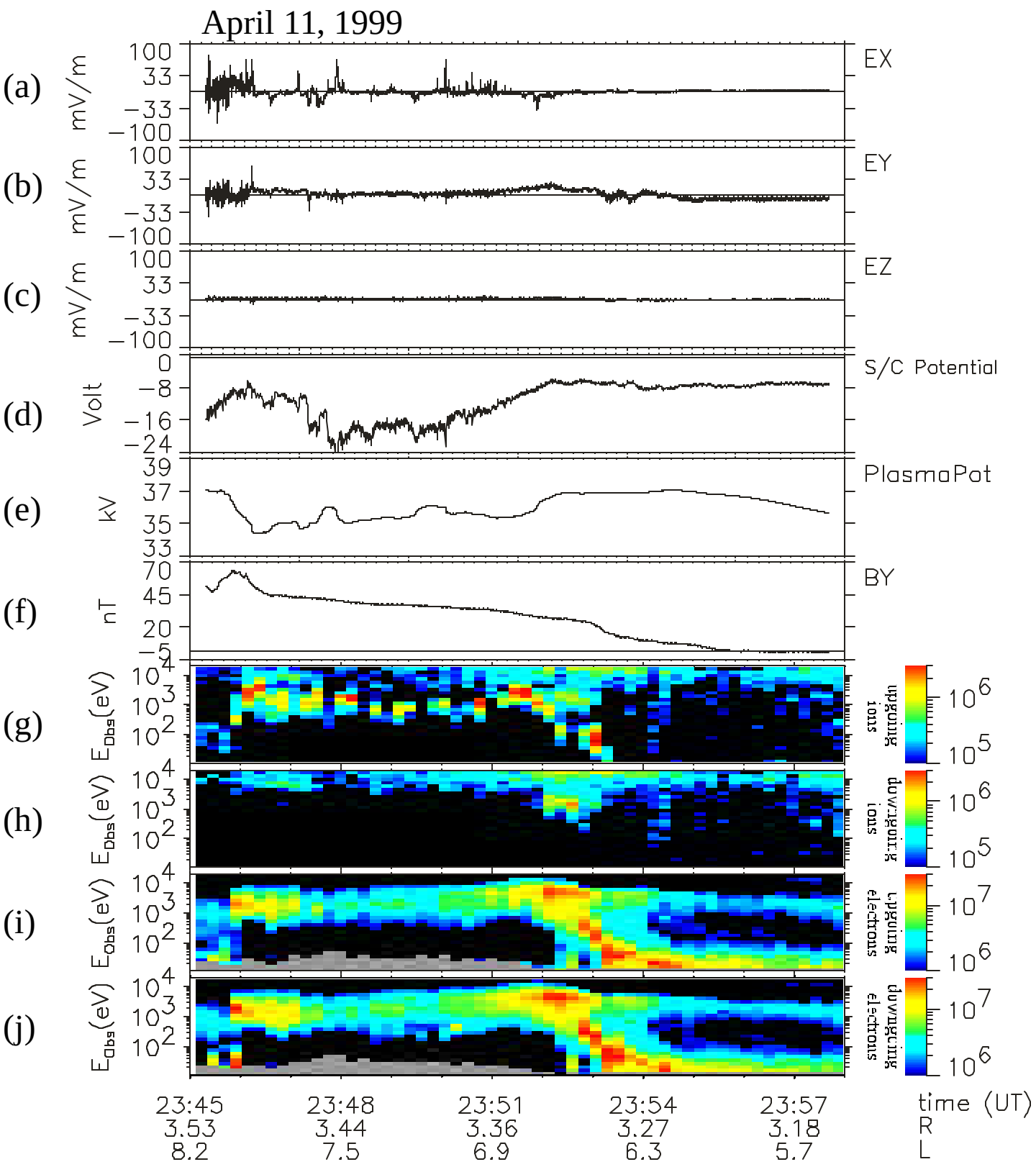
April 11, 1999
(a)
(b)
(c)
(d)
(e)
(f)
(g)
(h)
(i)
(j)
mV/m
EX
EY
EZ
Volt
S/C Potential
kV
PlasmaPot
nT
BY
E_Obs(eV)
upward ions
downward ions
upward electrons
downward electrons
23:45
3.53
8.2
23:48
3.44
7.5
23:51
3.36
6.9
23:54
3.27
6.3
23:57
3.18
5.7
time (UT)
R
L

Plate 7

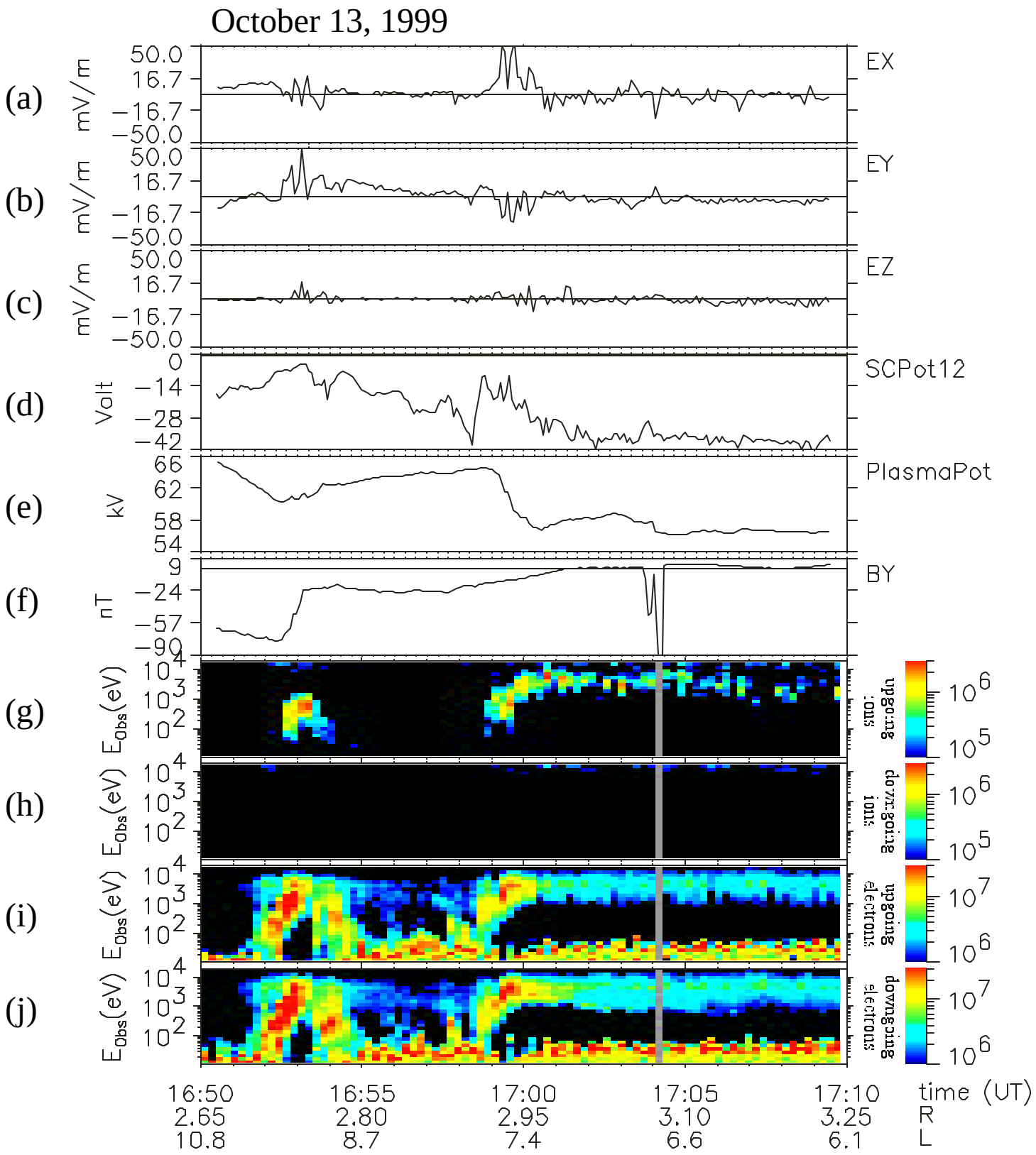
October 13, 1999
(a)
(b)
(c)
(d)
(e)
(f)
(g)
(h)
(i)
(j)
mV/m
50.0
16.7
−16.7
−50.0
EX
EY
EZ
Volt
0
−14
−28
−42
SCPot12
kV
66
62
58
54
PlasmaPot
nT
9
−24
−57
−90
BY
E_Obs(eV)
10^4
10^3
10^2
upgoing ions
downgoing ions
upgoing electrons
downgoing electrons
10^6
10^5
10^7
16:50
2.65
10.8
16:55
2.80
8.7
17:00
2.95
7.4
17:05
3.10
6.6
17:10
3.25
6.1
time (UT)
R
L

Plate 8

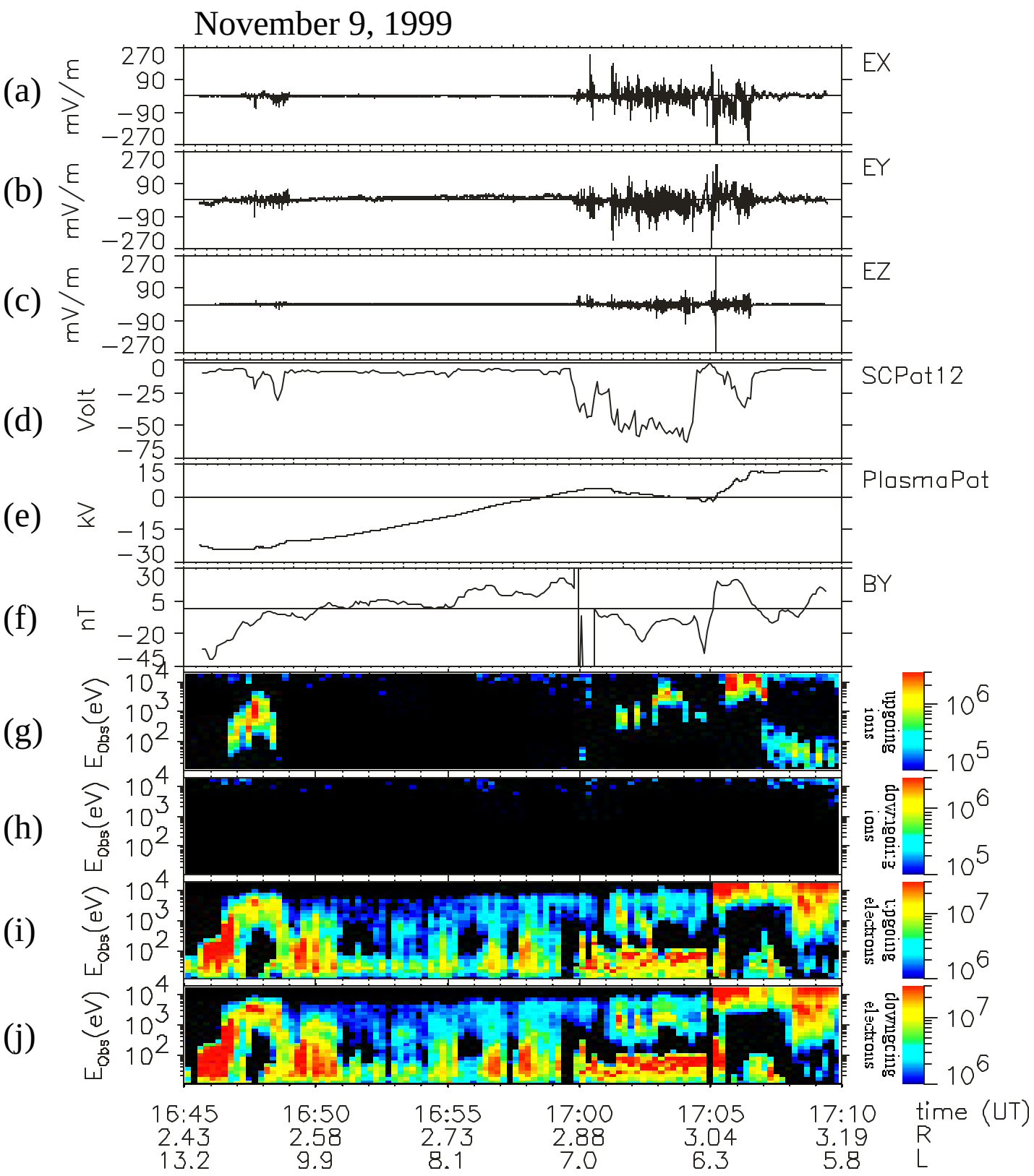
November 9, 1999
(a)
(b)
(c)
(d)
(e)
(f)
(g)
(h)
(i)
(j)
mV/m
Volt
kV
nT
EX
EY
EZ
SCPot12
PlasmaPot
BY
E_{Obs}(eV)
upgoing ions
downgoing ions
upgoing electrons
downgoing electrons
16:45 2.43 13.2
16:50 2.58 9.9
16:55 2.73 8.1
17:00 2.88 7.0
17:05 3.04 6.3
17:10 3.19 5.8
time (UT)
R
L

Plate 9